



Tunable spin-polarized transport through a side-gated double quantum dot molecular junction in the Coulomb blockade regime

Yebin Dai¹ · Xue-Feng Wang¹ · P. Vasilopoulos² · Yu-Shen Liu³

Received: 2 December 2018 / Accepted: 13 February 2019
© King Abdulaziz City for Science and Technology 2019

Abstract

Based on nonequilibrium Green's function method, we investigate spin-polarized transport properties of a side-gated double quantum dot (DQD) system in the Coulomb blockade regime under a magnetic field and an electric or thermal bias. The charge and spin currents oscillate frequently and can change sign upon varying gate voltage V_G if the electric bias is spin-dependent. Under a thermal bias, besides the charge- and spin-current oscillations with V_G , a pure spin current appears at the electron-hole symmetry point. Importantly, its sign can be controlled by the magnetic field above a "critical" strength. In addition, the charge- and spin-Seebeck coefficients oscillate nontrivially depending on V_G , B , and the tunnel coupling. Finally, we also study the spin-polarized transport properties of the DQD system effects under simultaneously applying an electric and a thermal bias.

Keywords Double quantum dots · Electric and thermal bias · Charge and spin currents · Coulomb blockade · Charge- and spin-Seebeck coefficients

Introduction

A quantum dot (QD) is a man-made sub-micron structure, which consists of 10^3 – 10^9 atoms and a comparable number of electrons. Its optical and electrical properties depend strongly on its size. When two QDs are joined into complex assemblies many opportunities are created for scientific discoveries (Alivisatos 1996; van der Wiel et al. 2002). As a result, QD systems have been widely investigated for many years (Beenakker et al. 1991; Baltin et al. 1999; Torres et al.

2003). The Kondo effect has been studied in both directly and indirectly coupled QDs (Sergueev et al. 2002; Jiang et al. 2005; Georges and Meir 1999; Büsser et al. 2000; Izumida and Sakai 2000; Aono and Eto 2001; Dong and Lei 2002; Aguado and Langreth 2000; López et al. 2002; Jeong et al. 2001; Chen et al. 2004; Zhang et al. 2005; Craig et al. 2004; Vavilov and Glazman 2005; Simon et al. 2005). QD molecular junctions have been predicted to exhibit strong thermal power due to the breakdown of the Wiedemann–Franz law and limited thermal conductance. It has been demonstrated that they exhibit a larger Seebeck effect due to the violation of the Wiedemann–Franz law and the weak phonon contribution to the thermal conductance (Yang et al. 2014; Liu et al. 2010, 2011; Hong et al. 2013; Zianni 2007; Liu and Yang 2010; Gómez-Silva et al. 2012). Besides, it has been found that Coulomb interaction might enhance the thermoelectric effect in QDs (Liu et al. 2010). Sun et al. coupled different types of spin batteries to the same QD to generate spin currents and found that dipolar batteries give results that are similar to yet different from those of unipolar devices (Wang et al. 2004). Hong et al. (2013) and Yang and Liu (2013) generated pure spin currents in a double QD (DQD) system by applying a thermal gradient to it in the presence (Hong et al. 2013) or absence (Yang and Liu 2013) of the intradot Coulomb interaction. Their results though are very

✉ Xue-Feng Wang
xf_wang1969@yahoo.com

Yebin Dai
790013487@qq.com

P. Vasilopoulos
p.vasilopoulos@concordia.ca

Yu-Shen Liu
ysliu@cslg.edu.cn

¹ School of Physical Science and Technology, Soochow University, 1 Shizi Street, Suzhou 215006, China

² Department of Physics, Concordia University, 7141 Sherbrooke Ouest, Montreal, QC H4B 1R6, Canada

³ College of Physics and Electronic Engineering, Changshu Institute of Technology, Changshu 215500, China

limited with respect to the side-gated voltage V_G (Yang and Liu 2013) and an applied magnetic field B . Accordingly, they missed the currents' oscillatory structure versus V_G and the fact that the pure spin current does not change sign above a tunnel-coupling-dependent threshold value of B . In addition, they have not evaluated the charge- and spin-Seebeck coefficients and have not considered the case of an electric and thermal bias applied simultaneously to the DQD.

In this work we couple a battery, or a spin-battery, and an electrical and/or thermal bias to a side-gated, by a potential V_G , DQD in the Coulomb blockade regime. We present extensive results for the charge and spin currents as functions of V_G , magnetic field, and tunnel coupling. In particular, we find that spin and charge currents can change sign under an electric bias and a pure spin current under a thermal bias. The latter changes sign above a tunnel-coupling-dependent threshold value of the magnetic field B .

We organize the paper as follows. In section "Model" we briefly describe the DQD system and introduce the non-equilibrium Green's function and some related formulas. In section "Results and discussion" we present numerical results for a DQD system subject to an electric or thermal bias and evaluate the corresponding charge- and spin-Seebeck coefficients. We also present results for the case of an electric and thermal bias applied simultaneously to the DQD. A summary follows in section "Summary".

Model

The system of the lead-DQD-lead in Fig. 1 can be described by Hamiltonian.

$$\hat{H} = \sum_{\beta,k,\sigma} \bar{\epsilon}_{\beta k} \hat{c}_{\beta k\sigma}^\dagger \hat{c}_{\beta k\sigma} + \sum_{\beta,k,\sigma} t_{\beta k} (\hat{d}_{\beta\sigma}^\dagger \hat{c}_{\beta k\sigma} + \text{h.c.}) + \sum_{\beta,\sigma} \epsilon_{\beta\sigma} \hat{d}_{\beta\sigma}^\dagger \hat{d}_{\beta\sigma} + \frac{E_c}{2} \sum_{\beta,\sigma} \hat{n}_{\beta\sigma} \hat{n}_{\beta\bar{\sigma}} + \sum_{\sigma} t_c (\hat{d}_{L\sigma}^\dagger \hat{d}_{R\sigma} + \text{h.c.}), \tag{1}$$

where $\hat{n}_{\beta\sigma} = \hat{d}_{\beta\sigma}^\dagger \hat{d}_{\beta\sigma}$ and $\beta = L, R$ represents the left and right leads or dots. $\hat{c}_{\beta k\sigma}^\dagger$ ($\hat{c}_{\beta k\sigma}$) and $\hat{d}_{\beta\sigma}^\dagger$ ($\hat{d}_{\beta\sigma}$) are the creation (annihilation) operators for electrons in the β electrode and QD, respectively, with spin index $\sigma = +1$ (\uparrow) or -1 (\downarrow). Further, $\bar{\epsilon}_{\beta k}$ is the electronic energy, as a function of the wave vector k in electrode β and $\epsilon_{\beta\sigma}$ the single-particle energy at the dots, which is spin degenerate in the absence of a magnetic field B . When such a field B is applied to the DQD device, we have $\epsilon_{\beta\sigma} = \epsilon_{\beta} - \sigma \epsilon_B/2$ with $\epsilon_B = 2\mu_B B$ the Zeeman splitting energy. A side-gate voltage V_G shifts $\epsilon_{\beta\sigma}$ and we set $\epsilon_L = \epsilon_R = V_G$. The charging energy due to the intradot Coulomb interaction is E_c . The factors $t_{\beta k}$ and t_c are the tunnel couplings and h.c. denotes the Hermitian conjugate term.

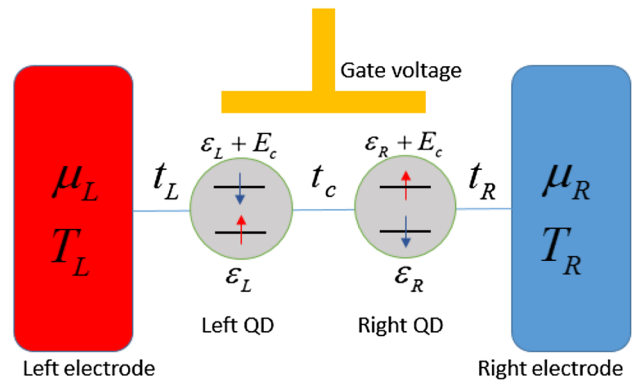


Fig. 1 A side-gated DQD coupled to a left (L) and a right (R) lead. The corresponding chemical potentials and temperatures are μ_L, μ_R , and T_L, T_R , respectively. E_c is each dot's charging energy and t_c the interdot tunnel coupling

We use the Green's function method to take into account the quantum coherence which can be neglected only in the limit of weak contact coupling between the dots and the electrodes (Beenakker et al. 1991; Baltin et al. 1999; Torres et al. 2003). In terms of the nonequilibrium Green's function the electron spin-dependent current I_σ is given by

$$I_\sigma = (1/2\pi) \int d\epsilon [f_{L\sigma}(\epsilon) - f_{R\sigma}(\epsilon)] \tau_\sigma(\epsilon), \tag{2}$$

where $f_{\beta\sigma}(\epsilon) = 1/\{\exp[(\epsilon - \mu_{\beta\sigma})/k_B T_\beta] + 1\}$ is the Fermi-Dirac distribution of electrons in the β lead, $\mu_{\beta\sigma}$ the chemical potential, and T_β the temperature. The transmission $\tau_\sigma(\epsilon)$ is given by $\tau_\sigma(\epsilon) = \text{Tr}[\Gamma_L G^r \Gamma_R G^a]_\sigma$, G^r (G^a) is the retarded (advanced) Green's function of the DQD, and $\Gamma_\beta = 2\pi \sum_k |t_{\beta k}|^2 \delta(\epsilon - \bar{\epsilon}_{\beta k})$ the linewidth function. The Green's functions of the whole system are obtained from the Dyson equation in the Keldysh formalism:

$$G^r(\epsilon) = g^r(\epsilon) + g^r(\epsilon) \Sigma^r G^r(\epsilon), \quad G^<(\epsilon) = G^r(\epsilon) \Sigma^<(\epsilon) G^a(\epsilon), \tag{3}$$

where g^r is the retarded Green's function of the isolated DQD system without coupling to the leads and $\Sigma^r, \Sigma^<$ are the self-energies. g^r is obtained by the equation-of-motion technique. Besides, the Hartree-Fock approximation is used for the higher-order Green's functions. It is reasonable when the temperature of the system is higher than the Kondo temperature (Haug and Jauho 2007). With $\epsilon_1 = \epsilon - \epsilon_{\beta\sigma}$ and $\epsilon_2 = \epsilon - \epsilon_{\beta\bar{\sigma}}, \bar{\beta} = R$ for $\beta = L, \bar{\beta} = L$ for $\beta = R$, we have

$$g_{\beta\beta}^r(\epsilon) = \frac{\epsilon_2(\epsilon_2 - E_c)[\epsilon_1 - E_c(1 - \langle n_{\beta\bar{\sigma}} \rangle)]}{D(\epsilon)}, \tag{4}$$

$$g_{\beta\bar{\beta}}^r(\epsilon) = \frac{t_c [\epsilon_1 - E_c(1 - \langle n_{\beta\bar{\sigma}} \rangle)][\epsilon_2 - E_c(1 - \langle n_{\bar{\beta}\bar{\sigma}} \rangle)]}{D(\epsilon)},$$

where

$$D(\epsilon) = \epsilon_1 \epsilon_2 (\epsilon_1 - E_c) (\epsilon_2 - E_c) - t_c^2 [\epsilon_1 - E_c (1 - \langle n_{\beta\bar{\sigma}} \rangle)] [\epsilon_2 - E_c (1 - \langle n_{\beta\sigma} \rangle)] \quad (5)$$

$$\Sigma^r = \frac{i}{2} \begin{pmatrix} -\Gamma_L & 0 \\ 0 & -\Gamma_R \end{pmatrix}, \quad \Sigma_\sigma^< = i \begin{pmatrix} \Gamma_L f_{L\sigma} & 0 \\ 0 & \Gamma_R f_{R\sigma} \end{pmatrix} \quad (6)$$

The electron occupation number $\langle n_{\beta\sigma} \rangle = \int d\epsilon \text{Im} G_{\beta\sigma}^<(\epsilon)/2\pi$ in the β QD for spin σ and its opposite $\bar{\sigma}$ can be calculated self-consistently.

In the linear response regime of a small voltage bias ΔV_σ and a small temperature difference ΔT between the electrodes we expand $\Delta f = f_L - f_R$ in a Taylor series and obtain $I_\sigma = G_0 K_{0\sigma}(\mu_\sigma, T) \Delta V_\sigma + G_0 K_{1\sigma}(\mu_\sigma, T) \Delta T / eT$ with $G_0 = e^2/h$ the conductance unit. The corresponding charge (S_c) and spin (S_s) Seebeck coefficients, for an open circuit $I_\sigma = 0$, are given by $S_c = (S_\uparrow + S_\downarrow)/2$ and $S_s = (S_\uparrow - S_\downarrow)/2$, respectively, with

$$S_\sigma = - \lim_{\Delta T \rightarrow 0} \frac{\Delta V_\sigma}{\Delta T} = - \frac{1}{eT} \frac{K_{1\sigma}(\mu_\sigma, T)}{K_{0\sigma}(\mu_\sigma, T)}, \quad (7)$$

$K_{\nu\sigma}(\mu_\sigma, T) = - \int d\epsilon [\partial f(\epsilon, \mu_\sigma, T) / \partial \epsilon] (\epsilon - \mu_\sigma)^\nu \tau_\sigma(\epsilon)$, and $\nu = 0, 1$. At low temperatures the Mott formula $S_\sigma \approx -(\pi^2 k_B^2 T / 3e) \tau'_\sigma(\mu_\sigma) / \tau_\sigma(\mu_\sigma)$ applies and can be used to obtain analytical results in simple cases.

Results and discussion

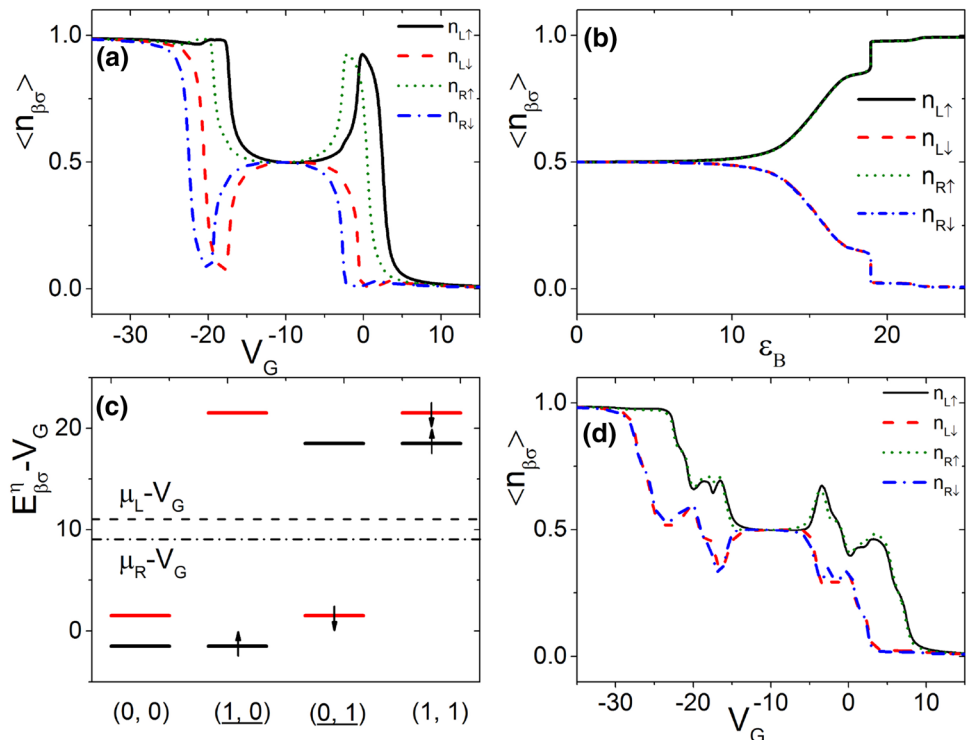
In the numerical calculations, we measure all energies in units of $\Gamma \equiv 0.1 \text{ eV}$ and use the energy-independent or wide-band approximation $\Gamma_L = \Gamma_R = \Gamma = \text{constant}$. The intradot Coulomb interaction energy is set to $E_c = 20\Gamma$. The total charge and spin currents are evaluated by $I_c = I_\uparrow + I_\downarrow$ and $I_s = I_\uparrow - I_\downarrow$, respectively.

Sign change of spin or charge current under an electric or spin bias

In this subsection we fix the temperature $k_B T_L = k_B T_R = 0.1 \Gamma$ and first consider the case in which the DQD is coupled to a spin-independent normal battery with $\mu_{L\uparrow} = \mu_{L\downarrow} = \Gamma$ and $\mu_{R\uparrow} = \mu_{R\downarrow} = -\Gamma$.

The system is similar to two independent one-state single-dots for weak t_c . In Fig. 2a we plot the average occupation number $\langle n_{\beta\sigma} \rangle$ versus the gate voltage V_G for weak inter-dot coupling $t_c = 0.1 \Gamma$ and a magnetic field B such that $\epsilon_B = 3\Gamma$. There appear two sets of single-dot curves separated by the electric bias $\Delta\mu = \mu_L - \mu_R = 2\Gamma$. The two dots are almost independent of each other. Their occupations depend on the Fermi energy and the temperature of the electrodes. The energy states in dot β read approximately $E_{\beta\sigma}^\eta = \epsilon_\beta - \sigma\epsilon_B/2 + \eta E_c$, with $\epsilon_\beta = V_G$, for $\eta = 0, 1$ due to the Coulomb blockade. A state gets occupied for $E_{\beta\sigma}^\eta < \mu_\beta$ or $V_G < \sigma\epsilon_B/2 - \eta E_c + \mu_\beta$; otherwise it is unoccupied.

Fig. 2 Occupation number $\langle n_{\beta\sigma} \rangle$ versus V_G at $\epsilon_B = 3\Gamma$ for **a** $t_c = 0.1 \Gamma$ and **d** $t_c = 5\Gamma$. $\langle n_{\beta\sigma} \rangle$ versus ϵ_B is shown in **b** for $V_G = -10\Gamma$ and $t_c = 0.1 \Gamma$. **c** Energy levels of each dot, measured from V_G , for weak $t_c = 0.1 \Gamma$ in the four possible spin-occupation (up, down) configurations. The dashed (dot-dashed) curve shows the chemical potentials of the left (right) electrode. $k_B T_L = k_B T_R = 0.1 \Gamma$, $\mu_L = \Gamma$, and $\mu_R = -\Gamma$ are assumed



There are four possible energy levels, i.e. $E_{\beta\uparrow}^0 - V_G = -1.5$, $E_{\beta\downarrow}^0 - V_G = 1.5$, $E_{\beta\uparrow}^1 - V_G = 18.5$, and $E_{\beta\downarrow}^1 - V_G = 21.5$ in each dot. The occupation configuration of spin (up, down) determines their levels as illustrated in Fig. 2c. The magnetic field breaks the spin symmetry and enhances greatly the occupation number of spin-up electrons in the dots. This Zeeman effect is sensitive when the chemical potential is near the levels $E_{\beta\sigma}^n$, corresponding to $V_G \approx -E_c = -20$ or $V_G \approx 0$, but less sensitive when $V_G \approx -E_c/2 = -10$. As a result, when the Zeeman energy $\epsilon_B = 3 \Gamma$ is small as indicated in Fig. 2a, the configuration (1, 0) dominates with $\langle n_{\beta\uparrow} \rangle \approx 1$ and $\langle n_{\beta\downarrow} \rangle \approx 0$ showing strong spin polarization near $V_G = -20$ or 0 but the configurations (0, 1) and (1, 0) appear with almost equal probabilities with $\langle n_{\beta\uparrow} \rangle \approx \langle n_{\beta\downarrow} \rangle \approx 0.5$ showing negligible spin polarization at $V_G = -10$. The spin polarization becomes significant even at $V_G = -10$ when the Zeeman energy is comparable to the Coulomb interaction, i.e. $\epsilon_B \geq 10 \Gamma$, and the probabilities of (0, 1) and (1, 0) differ greatly at finite temperature as shown in Fig. 2b.

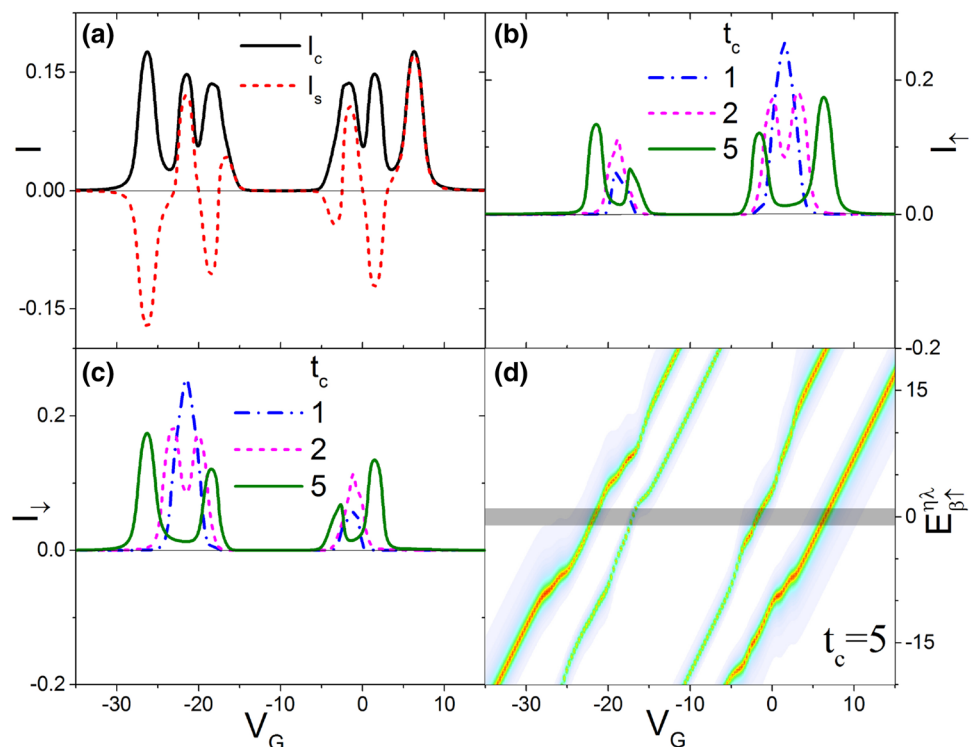
For large $t_c = 5 \Gamma$ in Fig. 2d, the system becomes similar to a single dot with two states. The difference of $\langle n_{\beta\sigma} \rangle$ in the two QDs (in the same QD), with the same (opposite) spin direction, vanishes (weakens). Each peak or step in the $\langle n_{\beta\sigma} \rangle$ -versus- V_G curve splits due to the split of the energy levels in the system.

In Fig. 3a we plot the charge and spin currents as functions of V_G in the presence of a magnetic field with $\epsilon_B = 3 \Gamma$ for $t_c = 5 \Gamma$. As shown, both currents exhibit an oscillatory structure for large negative and small positive values of

V_G and attain considerable values away from a “plateau” region in the range $-15 \Gamma \leq V_G \leq -5 \Gamma$. This spin current though changes its sign upon varying V_G . All these changes can be understood in terms of the up and down currents plotted in panels (b) and (c) for different t_c . Further confirmation comes from panel (d) in which the spin-up energy levels are shown as functions of V_G for $t_c = 5 \Gamma$. The dark bar denotes the transport window in which the electrons contribute to the current due to the chemical potential difference between the leads and the thermal energy. Their intersections with the energy levels correspond to the olive-colored peaks shown in panel (b). The numerical result indicates that the effective energy states in the system are approximately $E_{\beta\sigma}^{n\lambda} = \epsilon_\beta - \sigma \epsilon_B / 2 + \eta E_c + \lambda C_{\sigma\eta} t_c$ for $\lambda = \pm 1$ due to the inter-dot coupling. The inter-dot splitting is spin dependent in the presence of a magnetic field, $C_{\sigma\eta} = C_1$, for $(-1)^n \sigma = 1$, and $C_{\sigma\eta} = C_{-1}$ for $(-1)^n \sigma = -1$. In Fig. 3 we have $C_1 = C_{-1} = (0.04 \times |V_G + 12.6| + 0.204)$.

Due to the spin polarization effect presented in Fig. 2a for weak t_c and small ϵ_B , the spin-up (down) current is then suppressed at $V_G \approx -E_c = -20$ ($V_G \approx 0$) as shown in Fig. 3b, c (Wang et al. 2004). However, the inter-dot coupling makes the double-dot system qualitatively different from the one-state, single-dot case: t_c splits the two peaks of current for both spins and recovers partially the spin symmetry. Then, with reference to Fig. 3a we can see that the spin current will change its sign when V_G is changed by a small amount. This occurs because t_c modifies $\langle n_{\beta\sigma} \rangle$ as shown in Fig. 2d. Though not shown, similar observations of sign change apply to the

Fig. 3 **a** Charge current I_c versus V_G for $t_c = 5 \Gamma$. **b**, **c** Spin-up and spin-down currents, respectively, versus V_G for different tunnel couplings. **d** Shows the dot energy levels versus V_G and the horizontal dark bar denotes the transport window. The other parameters are $\epsilon_B = 3 \Gamma$, $k_B T_L = k_B T_R = 0.1 \Gamma$, and $\mu_L = \Gamma = -\mu_R$



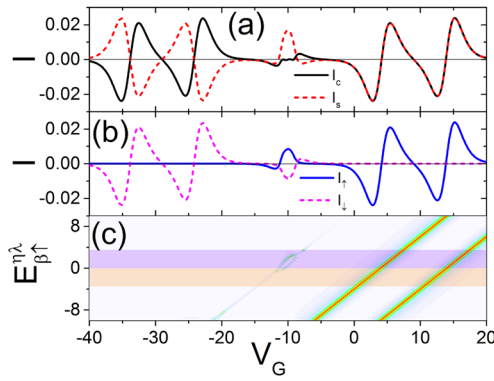


Fig. 4 **a** Charge I_c (solid curve) and spin I_s (dashed curve) current versus V_G . **b** I_{\uparrow} and I_{\downarrow} versus V_G . **c** Dot energy levels versus V_G . The purple (beige) horizontal band indicates the energy range with positive (negative) distribution difference $f_{L\sigma} - f_{R\sigma}$ in the transport window. Here $C_1 = 0.14$ and $C_{-1} = 0.86$. The other parameters are $\epsilon_B = 18 \Gamma$, $t_c = 5 \Gamma$, $k_B T_L = \Gamma$, $k_B T_R = 0.5 \Gamma$, and $\mu_L = \mu_R = 0$

charge current in a DQD coupled to a symmetric dipolar spin battery with $\mu_{L\uparrow} = \mu_{R\downarrow} = 1$ and $\mu_{L\downarrow} = \mu_{R\uparrow} = -1$.

Pure spin current generated by a thermal bias

We set $\mu_{L\uparrow} = \mu_{L\downarrow} = \mu_{R\uparrow} = \mu_{R\downarrow} = 0$, $k_B T_L = \Gamma$, $k_B T_R = 0.5 \Gamma$. For $\epsilon_B = 18 \Gamma$ and $t_c = 5 \Gamma$ in Fig. 4a we plot the total charge and spin currents and in Fig. 4b the spin-up and spin-down currents. The electron-hole symmetry point is at $V_G = -10 \Gamma$ (Hong et al. 2013). Due to the Coulomb blockade effect, the

states and transmission spectra for spin-up electrons are the mirror images of those for spin-down electrons with respect to the energy $\epsilon_m = V_G + E_C/2$, i.e. $T_{\uparrow}(\epsilon_m - E) = T_{\downarrow}(\epsilon_m + E)$. On the other hand, the Fermi distribution difference $\Delta f(\epsilon) = f_L(\epsilon, T_L) - f_R(\epsilon, T_R)$ between the two electrodes is an antisymmetric function with respect to the Fermi energy $\epsilon_F = 0$, that is, $\Delta f(\epsilon_F - E) = -\Delta f(\epsilon_F + E)$. At $V_G = -10 \Gamma$ we have $\epsilon_m = \epsilon_F = 0$ for $E_C = 20 \Gamma$ and the spin-up/down currents are opposite to each other, i.e., $I_{\uparrow} = \int_{-\infty}^{\infty} dE \Delta f(E) T_{\uparrow}(E) = -\int_{-\infty}^{\infty} dE \Delta f(E) T_{\downarrow}(E) = -I_{\downarrow}$. The total charge current vanishes and we have a pure spin current. In addition, the $\langle n_{\beta\sigma} \rangle$ and I_{σ} versus V_G curves for spin up are the rotational images of those for spin-down, that is, $\langle n_{\beta\sigma} \rangle(V_G) - 0.5 = 0.5 - \langle n_{\beta\bar{\sigma}} \rangle(-E_C - V_G)$ and $I_{\sigma}(V_G) = -I_{\bar{\sigma}}(-E_C - V_G)$, as shown in Figs. 2 and 4b.

We now investigate the dependence of I_s (i) on the magnetic field B and tunnel coupling t_c , for $V_G = -10 \Gamma$, and (ii) on V_G and B for fixed $t_c = 9 \Gamma$. The results for (i) are shown in Fig. 5a and those for (ii) in Fig. 5b. Panels (c) and (d) are cross sections of panels (a) and (b), respectively, for three values of t_c and ϵ_B . The oscillatory dependence of I_s on the magnetic field B and especially on V_G is evident in (a) and (b). In (a) the spin current attains one or two maxima, depending on t_c , and then decreases with ϵ_B , as the cross section in (c) confirms. Because of the aforementioned symmetry the charge current is always zero. Particularly interesting is the fact that the pure spin current becomes negative for $\epsilon_B > 20 \Gamma$ for all t_c shown and remains so for larger ϵ_B . Thus, by changing the field B one can control the sign of the

Fig. 5 **a** Spin current I_s versus magnetic field energy $\epsilon_B = \sigma B/2$ and tunnel coupling t_c but with fixed $V_G = -10 \Gamma$, $k_B T_L = \Gamma$, $k_B T_R = 0.5 \Gamma$, and $\mu_L = \mu_R = 0$. **b** Spin current I_s versus V_G and magnetic field energy ϵ_B . **c** Cross sections of **a** for different t_c . **d** Cross sections of **b** for different ϵ_B

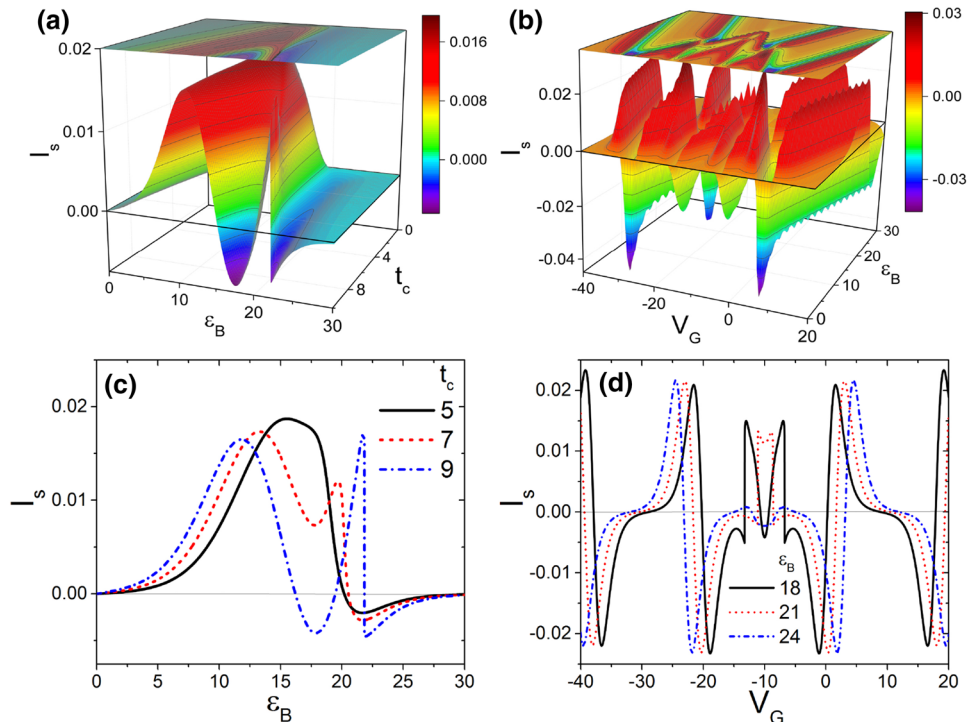
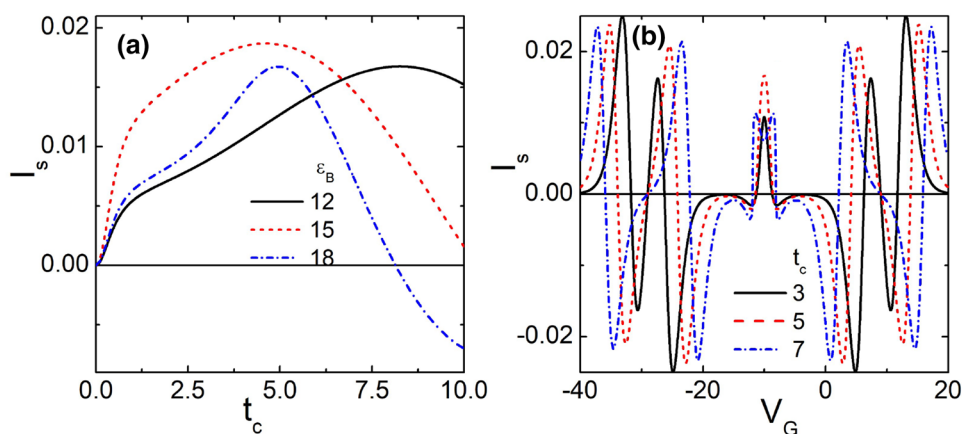


Fig. 6 a Spin current I_s versus tunnel coupling t_c for different ε_B but fixed $V_G = -10 \Gamma$. **b** I_s versus V_G for several tunnel couplings t_c but fixed $\varepsilon_B = 18 \Gamma$. The other parameters are: $k_B T_L = \Gamma$, $k_B T_R = 0.5 \Gamma$, $\mu_L = \mu_R = 0$



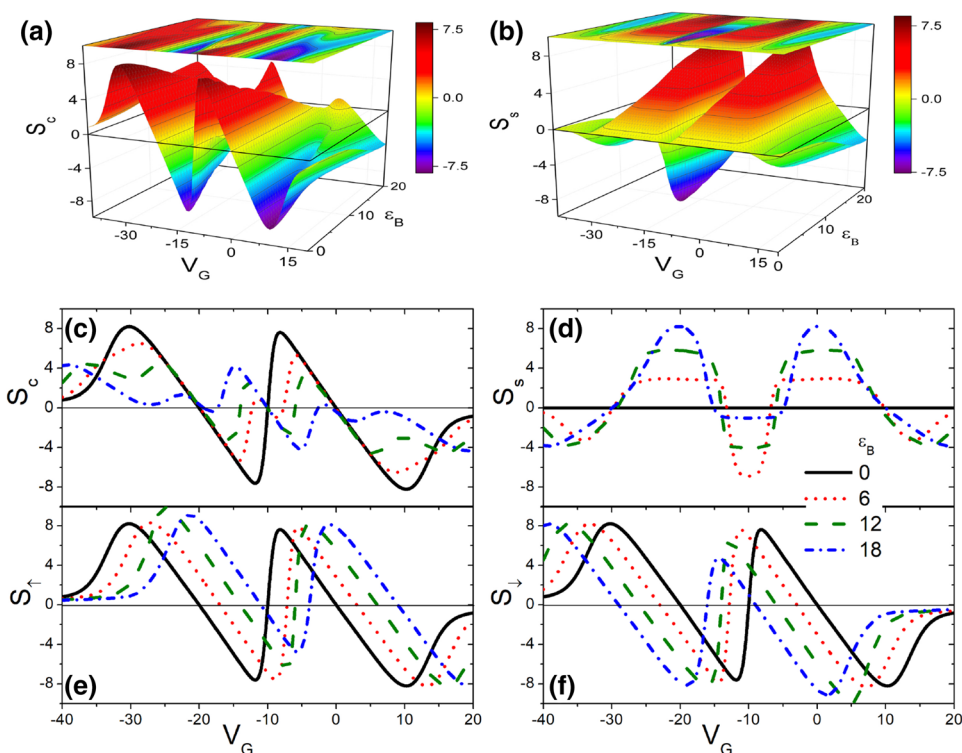
spin current. Further, Fig. 5d shows clearly the oscillatory dependence of I_s on V_G for three magnetic field energies ε_B . Such an oscillatory dependence, obviously not periodic, is absent in Refs. 15 and 21. It can be explained by a reasoning similar to that used for Fig. 4b.

The dependence of I_s on t_c is shown in Fig. 6a for different magnetic field energies ε_B but fixed $V_G = -10 \Gamma$, $k_B T_L = \Gamma$, $k_B T_R = 0.5 \Gamma$, $\mu_L = \mu_R = 0$. As seen, the spin current attains a maximum value and then slowly decreases with further increase of t_c . As for the charge current, it always vanishes because of the symmetry mentioned above. In Fig. 6b we show I_s versus V_G for several tunnel couplings t_c . Similar to

Fig. 5b, such an oscillatory structure is absent from Refs. 15 and 21.

We now turn our attention to the charge S_c and spin S_s Seebeck coefficients. We plot them versus V_G and magnetic field energy ε_B , respectively, in Fig. 7a, b, for fixed $t_c = 0.1 \Gamma$, $k_B T = \Gamma$, $\mu = 0$. Their oscillatory behavior with V_G is prominent in both of them. Panels (c) and (d) are cross sections of (a) and (b) at different ε_B as indicated. We notice split peaks in the S_c curve and up or down shifts of S_s as ε_B increases. We also notice that S_s vanishes for $\varepsilon_B = 0$. This behavior of S_c and S_s can be understood from the left shift of S_{\uparrow} and right shift of S_{\downarrow} shown in panels (e) and (f), respectively.

Fig. 7 a, b Charge S_c and spin S_s Seebeck coefficients versus V_G and magnetic field energy ε_B with fixed $t_c = 0.1 \Gamma$, $k_B T = \Gamma$, $\mu = 0$. **c, d** are, respectively, cross sections of **a, b** at different ε_B as indicated. For these ε_B panels **e** and **f** show the up (S_{\uparrow}) and down (S_{\downarrow}) components



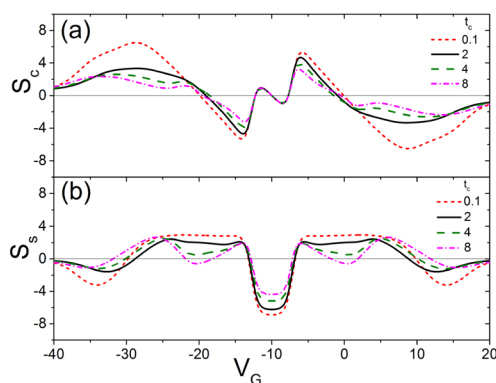


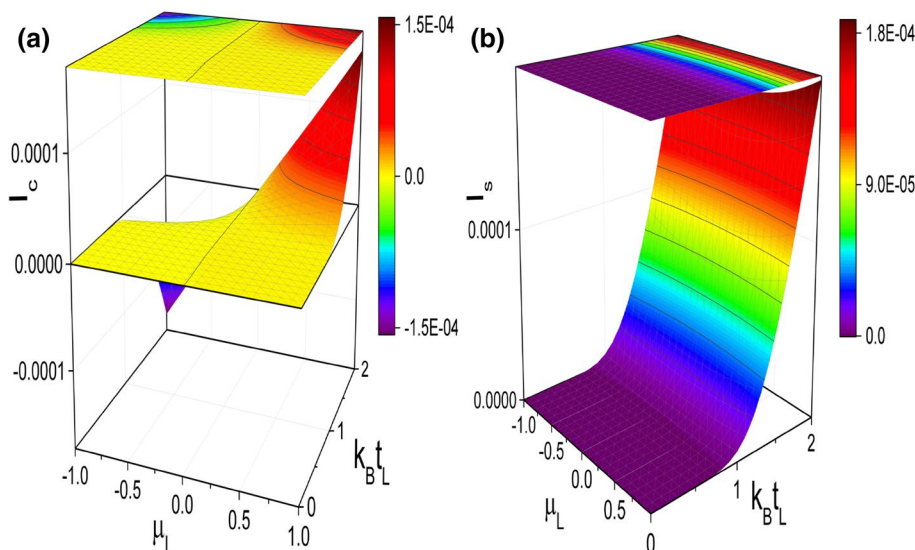
Fig. 8 **a** Charge I_c and **b** spin I_s Seebeck coefficients versus V_G for different tunnel couplings t_c but fixed $\epsilon_B = 6 \Gamma$, $k_B T = \Gamma$, $\mu = 0$

An oscillatory structure similar to that of Fig. 7 is shown in Fig. 8a, b where S_c and S_s are plotted versus V_G for different tunnel couplings t_c but fixed $\epsilon_B = 6 \Gamma$, $k_B T = \Gamma$, $\mu = 0$. We see that the oscillatory behavior is modified as t_c increases but it is not as uniform as when ϵ_B does.

Charge and spin currents under an electric and a thermal bias

Having considered the effect of each bias separately, one wonders what would be the combined effect of both biases applied simultaneously to the DQD. In Fig. 9a, b we plot, respectively, the charge I_c and spin I_s current versus $k_B T_L$ and μ_L for fixed $\epsilon_B = 3 \Gamma$, $t_c = 0.1 \Gamma$, $k_B T_R = 0.5 \Gamma$, and $\mu_R = 0$. As seen, for nearly all values of μ_L , the magnitudes of both I_c and I_s are mostly zero at small $k_B T_L$ and increase rapidly when $k_B T_L$ becomes significantly larger than $k_B T_R$. Note I_c changes signs with μ_L at large $k_B T_R$.

Fig. 9 **a** Charge I_c and **b** spin I_s current versus $k_B T_L$ and μ_L for fixed $\epsilon_B = 3 \Gamma$, $t_c = 0.1 \Gamma$, $k_B T_R = 0.5 \Gamma$, and $\mu_R = 0$



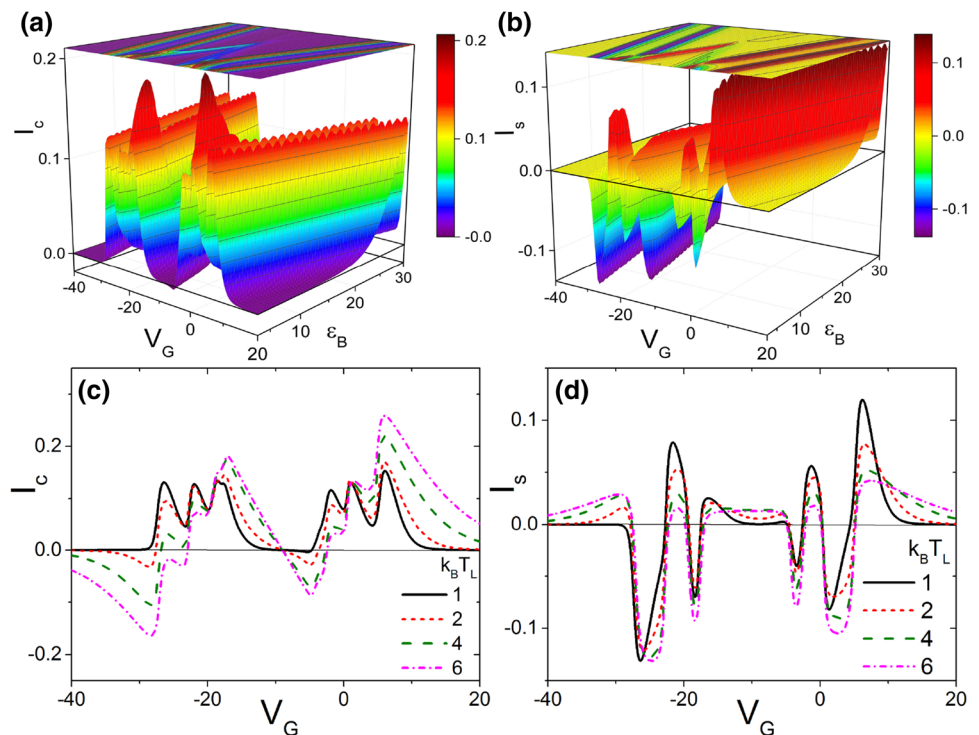
We also plot I_c , in Fig. 10a, and I_s in Fig. 10b, as functions of V_G and magnetic field energy ϵ_B for fixed $t_c = 5 \Gamma$, $k_B T_L = \Gamma$, $k_B T_R = 0.1 \Gamma$, $\mu_L = \Gamma$, and $\mu_R = -\Gamma$. Cross sections of (a) and (b), at $\epsilon_B = 3 \Gamma$, are shown in Fig. 10c, d, respectively, by the solid black curves; the other curves are for different $k_B T_L$ as indicated. Contrasting the results in (c) and (d) with those of Figs. 2 and 4, where, respectively, only an electric or thermal bias exists, one sees a rather significant difference as $k_B T_L$ increases. In particular, as $k_B T_L$ increases we see a progressive disappearance of the “plateau” region in Fig. 3 and an increase in the oscillation amplitude of I_c as well as the appearance of a plateau-like region in I_s at large thermal bias.

Summary

We studied a side-gated double-quantum-dot (DQD) system in the Coulomb blockade regime and in the presence of a magnetic field B . In the limit of weak inter-dot tunnel coupling t_c , the system behaves similar to two independent, one-state dots. With the increase of t_c , the degenerate levels of the two dots split and this results to current oscillations versus the side-gate voltage V_G for small positive or large negative values of V_G . The field B separates the current spectrum of opposite spins and significantly modulates the current oscillations. Under a normal electric bias the spin current changes sign upon varying V_G and so can the charge current if a spin-dependent bias is applied.

Charge- and spin-current oscillations versus V_G can also result from a thermal bias ∇T . In addition, ∇T can produce a pure spin current at the electron–hole symmetry point. Importantly, one can control the sign of this pure spin current by applying a field B of value above a “critical” one that depends on the tunnel coupling t_c . The charge-Seebeck

Fig. 10 **a** Charge current I_c and **b** spin current I_s versus V_G and magnetic field energy ϵ_B with fixed $t_c = 5 \Gamma$, $k_B T_L = \Gamma$, $k_B T_R = 0.1 \Gamma$, $\mu_L = \Gamma$, and $\mu_R = -\Gamma$. **c**, **d** the solid black curves are cross sections of **a**, **b**, at $\epsilon_B = 3 \Gamma$; the other curves are for different $k_B T_L$ as indicated



S_c and spin-Seebeck S_s coefficients can then oscillate non-trivially depending on the voltage V_G , the tunnel coupling t_c , and the field B .

Finally, we explored the effect of simultaneously applying an electric and a thermal bias to the DQD and presented some results for the charge I_c and spin I_s currents versus biases or V_G . Relative to the single-bias case significant changes occur in the results when the thermal bias is strengthened, e.g., the oscillation amplitude of I_c increases and a plateau-like region in I_s appears at large thermal bias.

Acknowledgements This work was supported by National Natural Science Foundation of China (Grant Nos 61674110 and 91121021 and 6167204) and by the Canadian NSERC Grant No. OGP0121756.

Compliance with ethical standards

Conflict of interest None of the authors of this manuscript have any competing interests.

References

- Aguado R, Langreth DC (2000) Out-of-equilibrium Kondo effect in double quantum dots. *Phys Rev Lett* 85:1946
- Alivisatos P (1996) Semiconductor clusters, nanocrystals, and quantum dots. *Science* 271:5251
- Aono T, Eto M (2001) Kondo resonant spectra in coupled quantum dots. *ibid* 63:125327
- Baltin R, Gefen Y, Hackenbroich G, Weidenmüller HA (1999) Correlations of conductance peaks and transmission phases in deformed quantum dots. *Eur Phys J B*. 10:119
- Beenakker WJ (1991) Theory of Coulomb-blockade oscillations in the conductance of a quantum dot. *Phys Rev B*. 44:1646
- Büscher CA, Anda EV, Lima AL, Davidovich MA, Chiappe G (2000) Transport in coupled quantum dots: kondo effect versus anti-ferromagnetic correlation. *Phys Rev B*. 62:9907
- Chen JC, Chang AM, Melloch MR (2004) Transition between quantum states in a parallel-coupled double quantum dot. *Phys Rev Lett* 92:176801
- Craig NJ, Taylor JM, Lester EA, Marcus CM, Hanson MP, Gossard AC (2004) Tunable non-local spin control in a coupled quantum dot system. *Science* 304:565
- Dong B, Lei XL (2002) Kondo effect and anti-ferromagnetic correlation in transport through tunneling-coupled double quantum dots. *ibid* 65:241304(R)
- Georges, Meir Y (1999) Electronic correlations in transport through coupled quantum dots. *Phys Rev Lett*. 82:3508
- Gómez-Silva G, Avalos-Ovando O, Ladrón de Guevara ML, Orellana PA (2012) Enhancement of thermoelectric efficiency and violation of the Wiedemann-Franz law due to Fano effect. *J Appl Phys* 111:053704
- Haug H, Jauho AP (2007) Quantum kinetics in transport and optics of semiconductors, 2nd edn. Springer, Berlin
- Hong XK, Liu YS, Feng JF, Chu JH (2013) Thermal spin current through a double quantum dot molecular junction in the Coulomb blockade regime. *J Appl Phys* 114:144309
- Izumida W, Sakai O (2000) Two-impurity Kondo effect in double-quantum-dot systems—effect of interdot kinetic exchange coupling. *ibid*. 62:10260
- Jeong H, Chang AM, Melloch MR (2001) The Kondo effect in an artificial quantum dot molecule. *Science*. 293:2221
- Jiang Z, Sun Q, Wang Y (2005) Kondo transport through serially coupled triple quantum dots. *Phys Rev B* 72:045332

- Liu YS, Yang XF (2010) Enhancement of thermoelectric efficiency in a double-quantum-dot molecular junction. *J. Appl Phys* 108:023710
- Liu J, Sun Q-F, Xie XC (2010) Enhancement of the thermoelectric figure of merit in a quantum dot due to the Coulomb blockade Effect. *Phys Rev B*. 81:245323
- Liu YS, Zhang DB, Yang XF, Feng JF (2011) The role of Coulomb interaction in thermoelectric effects of an Aharonov–Bohm interferometer. *Nanotechnology* 22:225201
- López R, Aguado R, Platero G (2002) Nonequilibrium transport through double quantum dots: Kondo effect versus antiferromagnetic coupling. *Ibid* 89:136802
- Sergueev N, Qing-Feng S, Guo H (2002) Spin-polarized transport through a quantum dot: Anderson model with on-site Coulomb repulsion. *Phys Rev B* 65:165303
- Simon P, López R, Oreg Y (2005) RKKY and magnetic field interactions in coupled Kondo quantum dots. *Phys Rev Lett* 94:086602
- Torres LEFF, Lewenkopf CH, Pastawski HM (2003) Coherent versus sequential electron tunneling in quantum dots. *Phys Rev Lett*. 91:116801.
- van der Wiel WG, De Franceschi S, Elzerman JM et al (2002) Electron transport through double quantum dots. *Rev Mod Phys*. 75:1.
- Vavilov MG, Glazman LI (2005) Transport spectroscopy of Kondo quantum dots coupled by RKKY interaction. *Phys Rev Lett* 94:086805
- Wang D-K, Sun Q-F, Guo H (2004) Spin-battery and spin-current transport through a quantum dot. *Phys Rev B* 69:205312
- Yang XF, Liu YS (2013) Pure spin current in a double quantum dot device generated by thermal Bias. *J Appl Phys* 113:164310
- Yang Z-C, Sun Q-F, Xie XC (2014) Spin-current Seebeck effect in quantum dot systems. *J Phys Condens Matter* 26:045302
- Zhang GM, Lu R, Liu ZR, And L, Yu (2005) Swapping Kondo resonances in coupled double quantum dots. *Phys Rev B* 72:073308
- Zianni X (2007) Coulomb oscillations in the electron thermal conductance of a dot in the linear regime. *Phys Rev B* 75:045344

Publisher's Note Springer Nature remains neutral with regard to jurisdictional claims in published maps and institutional affiliations.

Reproduced with permission of copyright owner. Further reproduction prohibited without permission.